09

Quality Factor of Micro-ring Resonators: Calculation Method and Experiment

© D.E. Artemov,[1,2] A.V. Buchinskii,[3] A.P. Smirnov,[2] A.A. Ershov,[4] A.A. Nikitin,[4] A.B. Ustinov,[4]
V.H. Treshikov,[1] A.I. Fedoseev[2]

[1]T8 LLC, Moscow, Russia
[2]Moscow State University, Moscow, Russia
[3]Moscow Institute of Physics and Technology (National Research University), Dolgoprudny, Moscow Region, Russia
[4]St. Petersburg Electrotechnical University „LETI“, St. Petersburg, Russia
e-mail: artemov.de@t8.ru

Received October 2, 2024
Revised December 13, 2024
Accepted December 21, 2024

A model for calculation of the loaded quality factor of a micro-ring resonator, which takes into account distributed coupling of the ring with a straight waveguide, has been developed. A numerical simulation of the loaded Q-factor was performed for micro-ring resonators with specified geometry and refractive index profiles. The modeling results were compared with experimental Q-factor values derived from the measured transmission characteristics of micro-ring resonators with various geometries. To the authors' knowledge, the obtained satisfactory agreement between theoretical and experimental data has been demonstrated for the first time. This validates the proposed model and method for preliminary calculations and the design of high-Q micro-ring resonators.

Keywords: microring resonator, quality factor, coupled mode theory, Fabry-Perot interferometer.

DOI: 10.61011/TP.2025.06.61383.308-24

Introduction

Today, micro-ring resonators (MRR) are the key elements of photonic integrated circuit. Such elements are used as various passive devices, as well as compact and broadband electrooptic modulators [1]. It should be noted that due to lowering the thresholds of nonlinear effects [2] MRR are used in fabrication of various nonlinear devices [3]. One of the key characteristics of MRR is its quality factor (Q-factor), which is determined by both the light decay in the waveguide and the losses caused by the coupling of the MRR modes and the input waveguides. From the light attenuation coefficient in the waveguide, it is possible to calculate the intrinsic Q-factor of MRR with a given geometry [4]. The coupling-induced losses are determined by the energy exchange between the longitudinal modes of MRR and the modes of the nearby waveguides [5]. To evaluate the loaded Q-factor of MRR, first of all, it is necessary to calculate the characteristics of the longitudinal modes of the waveguides. These characteristics are calculated, as a rule, using well-known approaches (see, for example, [6]) based on solving the two-dimensional Helmholtz equation [7].

At the same time, the calculation of energy exchange between modes in the coupling region, which is a more complex task, can be performed based on a coupled-mode theory [8–12] by analogy with a similar task in the microwave range [13] or within the model with 3-dimensional wave equation [14,15]. Efficient numerical calculation methods within the framework of the latest model, such as FDTD, are implemented in commercial software [6]. In this regard, it should be noted that in the literature there is no comparison of the results of such calculations with experimental data for the high-Q MRR. Because the software is inaccessible, it can only be assumed that errors in calculation of optical losses and coupling of the waveguide modes may occur during sampling of the model.

In this paper, we propose a simplified model for calculating the loaded Q-factor of the high-Q MRR. The model is based on multipath interference of partial waves circulating in the MRR. At that, at each transition the energy exchange is considered within the coupled-mode theory. Due to the latter theory the calculation may be reduced to a one-dimensional analysis. The adequacy of this approach is verified by comparing it with experimentally obtained transmission spectra of four MRR samples. The data obtained allowed us to conclude that within each resonance, the MRR transmission spectrum has the same profile as the Fabry-Perot interferometer.

1. Eigen longitudinal modes of MRR and straight waveguide

MRR with a near coupling element — section of the straight waveguide — shown in Fig. 1. The table below shows the values of the geometric parameters of the samples. The refractive index of the core (Si_3N_4) and cladding (SiO_2) materials of the rectangular waveguide were obtained from the manufacturer of the photonic integrated circuit.

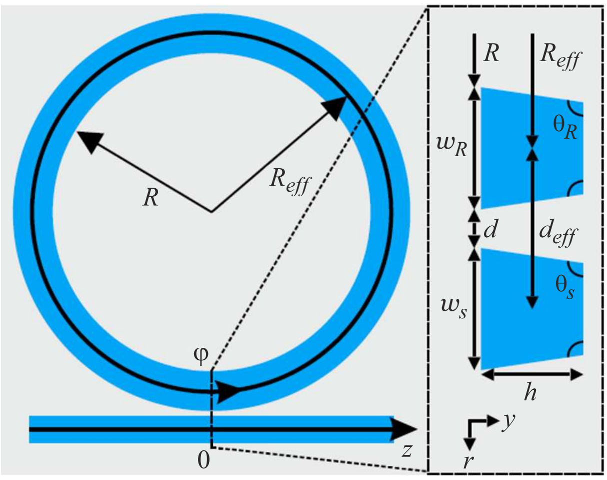

Figure 1. Geometry of the studied MRR and coupling element — section of the straight waveguide.

Values of the parameters used in the calculation model

R	w_R	w_S	h	d
250.18	1	1	0.8	0.4–0.6

Note. All values are given in μm.

Due to the symmetry and uniformity of geometry, the electric field components of the longitudinal eigenmodes $\vec{E}_R$ of MRR and $\vec{E}_{WG}$ of the straight waveguide are generally represented by the product of amplitudes A_R and B_{WG}, real valued transverse field distributions e_R and e_{WG} and phase multipliers:

$$\begin{cases} E_R^{(q)}(r, y, \phi, t) = A_R(\varphi) \cdot e_R^{(q)}(r, y) \\ \quad \times \exp\left\{i \cdot \left(\varphi_R^{(q)} + \omega t - m_R \phi\right)\right\}, q = r, y, \phi, \\ E_{WG}^{(q)}(x, y, z, t) = B_{WG}(z) \cdot e_{WG}^{(q)}(x, y) \\ \quad \times \exp\left\{i \cdot \left(\varphi_{WG}^{(q)} + \omega t - \beta_{WG} z\right)\right\}, q = x, y, z. \end{cases} \tag{1}$$

The values m_R, β_{WG} and $\vec{e}_R, \vec{e}_{WG}$ in (1) are found as eigen values and eigen functions of the wave equation for the purpose of which in this paper the solver ARPACK is used as a part of module Electromagnetic Waves, Frequency Domain (software „COMSOL Multiphysics").

Figure 2, a shows the calculated distribution of Umov-Poynting vector component $P^{(\phi)}|_{\lambda=1.55\,\mu\text{m}}$ for the waveguide longitudinal modes of MRR. The numbers of the longitudinal modes are given by m_R. In the considered case, the geometry of the waveguide provides propagation of only 4 waveguide modes (the black arrows define the vector $\vec{e}_R(r, y)$ in the plane of the figure). The modes with $j = 1, 2$ are further referred to as fundamental (lower-order modes), while the remaining modes are — non-fundamental (higher-order modes). The two fundamental modes correspond to two orthogonal polarizations.

Figure 2, b shows the dispersion of the propagation constant $\beta_R = m_R/R_{\text{eff}}$ of the longitudinal MRR modes in the wavelength range 1520–1620 nm. Here

$$R_{\text{eff}} = \frac{\iint r P^{(\phi)}\, drdy}{\iint P^{(\phi)}\, drdy}$$

— effective MRR radius, which at relatively small values R coincides with the distance from the MRR center to the middle point of the MRR waveguide $R_{\text{eff}} \approx R + w_R/2$ (see Fig. 1).

It is convenient to call as quasi-TE modes such of the listed modes, the vector $\vec{e}$ of which in cross-section is directed mainly along the largest of the sides of the waveguide (in this case — along the horizontal axis r). While quasi-TM modes — are such that the magnetic field strength vector $\vec{h}$ is directed predominantly along the largest of the sides of the waveguide (in this case, the vector $\vec{e}$ is directed predominantly along the smallest of the sides of the waveguide — along the axis y). In this case the quasi-TE modes — are the modes with $j = 1, 4$, quasi-TM modes — are the modes with $j = 2, 3$.

Calculations show that with the selected radius of MRR and the cross section of the waveguides, the field distributions and propagation constants of the corresponding quasi-TE and TM modes of MRR and straight waveguide are approximate in magnitude. Note that as the radius of the ring decreases, the difference between them will be greater.

Next, the results shown in Fig. 2 will be used to calculate the energy exchange between the longitudinal modes of MRR and the nearby straight waveguide.

2. Coupling of the longitudinal modes of MRR and straight waveguide

The interaction of the longitudinal modes leads to the transfer of optical energy from MRR to the straight waveguide and back [5,9], accompanied by a change in the

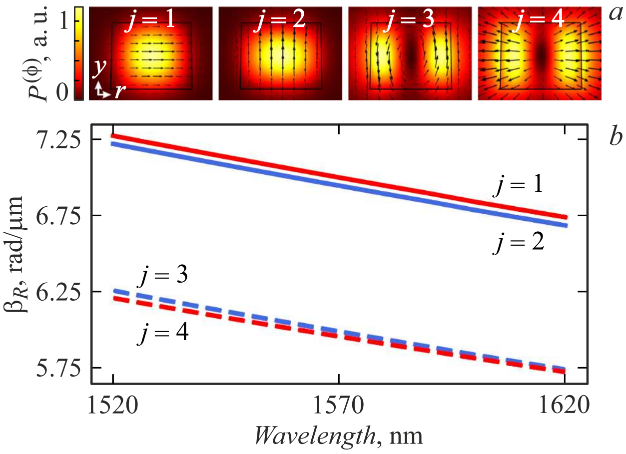

Figure 2. Numerical modeling results. (a) Intensity distribution and (b) dispersion of the propagation constant β_R of the eigen longitudinal modes of MRR.

amplitude of the fields $\vec{E}_R(r,y,\phi)$ and $\vec{E}_{WG}(x,y,z)$ along z axis. In case of weak coupling, which is typical for high-Q MRR, we describe the phenomenon of energy exchange by equations obtained within the coupled-mode theory [9]. According to this theory, the interaction is considered to change only the amplitudes of the coupled modes $A_R(\varphi)$ and $B_{WG}(z)$, leaving unchanged their transverse distributions of field $e_R(r,y)$, $e_{WG}(x,y)$ and propagation constants β_R and β_{WG}. The use of a large bending radius of MRR allows for a one-to-one correspondence of the interacting wavefronts of the longitudinal modes [16]. The existence of non-fundamental modes is not taken into account, since these modes decay much faster than the fundamental ones due to their greater overlap with the roughness of the dielectric waveguide boundaries. The equations for complex amplitudes $\tilde{A}_R$ and $\tilde{B}_{WG}$ are used to describe the coupling of identical single-mode parallel waveguides without attenuation [16,17]:

$$\begin{cases} \frac{d}{dz}\tilde{A}_R(z) = -i\beta_R^{(z)}(z)\cdot\tilde{A}_R(z) + iC(z)\cdot\tilde{B}_{WG}(z), \\ \frac{d}{dz}\tilde{B}_{WG}(z) = -i\beta_{WG}\cdot\tilde{B}_{WG}(z) + iC^*(z)\cdot\tilde{A}_R(z), \\ \tilde{A}_R(z) \equiv A_R(z)\cdot e^{-i\beta_R^{(z)}(z)\cdot z}, \\ \tilde{B}_{WG}(z) \equiv B_{WG}(z)\cdot e^{-i\beta_{WG}\cdot z}. \end{cases} \tag{2}$$

Here $C(z)$ — the overlap integral of the transverse distributions of the longitudinal mode of MRR and the mode of the straight waveguide; i — imaginary unit; $*$ — complex conjugation; $\beta_R^{(z)}(z)$ — projection onto z axis of the propagation constant β_R of MRR longitudinal mode. In the absence of coupling ($C(z)\equiv 0$), these equations describe the phase change of the complex amplitude along z axis. Because the modes are coupled it leads to a periodic change in the complex amplitudes of the interacting modes. The complex-valued coefficient $C(z)$ characterizes the rate of energy exchange. The above system of equations describes the relationship between the identically polarized fundamental longitudinal modes of MRR and the waveguide and is similar in form to the equations of coupled modes for two identical straight waveguides. The above equations differ from [16,17] in that the parameters $C(z)$ and $\beta_R^{(z)}(z)$ clearly depend on z. This allows us to describe the connection of non-parallel waveguides in a simplified formalism of parallel waveguides.

Parameter $\beta_R^{(z)}(z)$ may be approximated by the expression [16,17]:

$$\beta_R^{(z)}(z) \approx \beta_R\cdot\left[1 - \frac{d_{\text{eff}}}{R_{\text{eff}}} - \left(\frac{z}{2R_{\text{eff}}}\right)^2\right]^2. \tag{3}$$

Here d_{eff} is the distance between the centers of the transverse field distributions of the longitudinal MRR mode and the straight waveguide mode. For a relatively large radius R, the parameter d_{eff} coincides with the distance between the centers of the waveguides, as shown in Fig. 1.

The calculation of the overlap integral $C(z)$ in case of weak coupling of the bending and straight waveguides is simplified by two assumptions.

First, in $z=0$ plane, the wavefronts of the longitudinal modes are strictly parallel to each other, therefore, within the framework of the well-known formalism for two coupled identical single-mode parallel waveguides [9]:

$$C(0) = \frac{\begin{gathered}\frac{k_0}{4}\sqrt{\frac{\epsilon_0}{\mu_0}}\iint\limits_{S_{WG}}\left(n_{core}^2 - n_{clad}^2\right)\cdot\left(\tilde{e}_R^{(r)^*}\cdot\tilde{e}_{WG}^{(x)} + \right. \\ \left. + \tilde{e}_R^{(y)^*}\cdot\tilde{e}_{WG}^{(y)} + \left(\frac{n_{clad}}{n_{core}}\right)^2\tilde{e}_R^{(\phi)^*}\cdot\tilde{e}_{WG}^{(z)}\right)dS\end{gathered}}{\sqrt{\iint P_R^{(\varphi)}\,drdy}\cdot\sqrt{\iint P_{WG}^{(z)}\,dxdy}}. \tag{4}$$

Here $k_0 = 2\pi/\lambda$ — wavenumber at wavelength λ in vacuum; ϵ_0, μ_0 — electric and magnetic constants in vacuum; n_{core}, n_{clad} — core and cladding refractive indices at wavelength of λ; S_{WG} — the core region of the straight waveguide.

Secondly, it is assumed that MRR's coupling region consists of separate pieces parallel to the straight waveguide and located at different distances from the straight waveguide. Therefore, at $z\neq 0$ ($\varphi\neq 0$), the coefficient $C(z\neq 0)$ decreases in comparison with $C(0)$ only due to an increase in the gap between the interacting regions of MRR and straight waveguide. Since the field decays outside the core of the waveguide according to the law $E(r)\propto e^{-\gamma r}\approx e^{-\gamma z^2/2R_{\text{eff}}}$ [9,17,18], approximate expressions can be written for $C(z)$ [17,18]:

$$\begin{cases} C(z) = C(0)\cdot e^{-\gamma z^2/2R_{\text{eff}}}, \\ \gamma = \frac{\gamma_R + \gamma_{WG}}{2}, \\ \gamma_{R,WG} = \sqrt{\beta_{R,WG}^2 - (n_{clad}\cdot k_0)^2}. \end{cases} \tag{5}$$

Figure 3 shows the results of solving the system of equations (2) for a quasi-TE mode with parameters described in the ratios (3)–(5), at a wavelength of $\lambda = 1.55\,\mu$m at a gap of $d = 0.5\,\mu$m and with the following conditions on the left border of the coupling region ($2L = 80\,\mu$m — the length of the calculated area and the estimated length of the coupling region)

$$\begin{cases} A_R(-L) = 1, \\ B_{WG}(-L) = 0. \end{cases} \tag{6}$$

From the graphs we may see that the coupling region of longitudinal modes doesn't exceed $60\,\mu$m ($\approx 5\%$ of MRR length) for the given geometry.

When substituting the analytical expressions for the coefficients $\beta_R^{(z)}(z)$ and $C(z)$ into equations (3) and (5), respectively, the effective values of the parameters $d_{\text{eff}} = 1.48\,\mu$m and $R_{\text{eff}} = 250.69\,\mu$m are used. The difference between the effective and geometric values is negligible compared to the selected radius of MRR, but it rises with the lower radius of MRR.

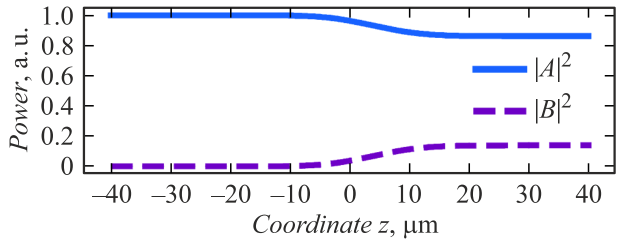

Figure 3. Distribution of the normalized powers of the fundamental quasi-TE mode of MRR (continuous line) and straight waveguide (dashed line) along the coupling region. z axis is shown in Fig. 1.

The result of calculations (2)–(6) is the amplitude transmission coefficient t of the coupling region.

$$t = \left| \frac{A_R(L)}{A_R(-L)} \right|. \tag{7}$$

The calculated value of t is further used in the analysis of multipath interference in MRR.

3. Multi-beam interference in MRR

The amplitude E_{th} of the transmitted wave is formed as a result of multipath interference of partial waves inside MRR when continuous radiation is injected into a waveguide with an amplitude of E_{in} (Fig. 4). The initial ($n = 0$, where n is a number of the wave circulations) wave $E_p^0 = ikE_{in}$ propagating in MRR is the result of energy flowing in the coupling region from the longitudinal mode E_{in} of the straight waveguide into the longitudinal mode of MRR. After a single round trip over the MRR, the initial wave transforms into a wave with index $n = 1$ and an amplitude $E_p^1 = E_p^0 \cdot \exp\{-\alpha L_R/2 - i\beta_R L_R\} \cdot t$, determined by the attenuation α (in power), phase incursion $\beta_R L_R$ of the longitudinal mode in MRR with the lenght of L_R and the amplitude transmission ratio t of the coupling region. As a result, there are two waves in MRR at the output of the coupling region after the first wave transmission - E_p^1 and E_p^0 (the existence of E_p^0 is provided by continuous pumping). After $n = 0 \ldots \infty$ transmissions $n + 1$ partial longitudinal modes of MRR are propagating in MRR with the same transverse distribution, the complex amplitude $E_p^n = E_p^{n-1} \cdot \exp\{-\alpha L_R/2 - i\beta_R L_R\} \cdot t$ of which

$$E_p^n = E_p^0 \cdot \left[t \cdot a \cdot e^{-i\theta}\right]^n, \; a = e^{-\alpha L_R/2}, \; \theta = \beta_R L_R.$$

The resulting field E inside MRR is the sum of partial waves, the existence of which is ensured by continuous pumping of the wave E_p^0:

$$E(\theta) = \sum_{n=0}^{\infty} E_p^n = \frac{E_p^0}{1 - ate^{-i\theta}}.$$

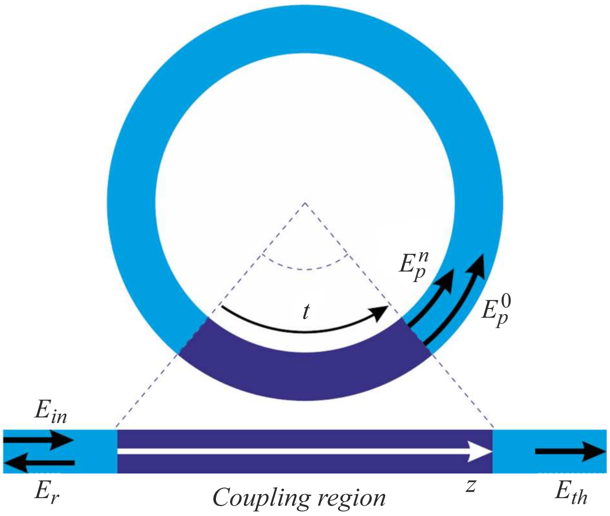

Figure 4. The coupling of the complex amplitudes of the longitudinal mode in different regions of MRR.

The intensity of field I inside MRR is determined by the square of the amplitude modulus of the resulting field

$$I(\theta) = |E|^2 = \frac{I_m}{1 + \left(\frac{2F}{\pi}\right)^2 \sin^2\frac{\theta}{2}}, \; I_m = \frac{\left|E_p^0\right|^2}{(1 - at)^2}. \tag{8}$$

In resonance ($\theta_m = 2\pi m$, m — integer), the intensity $I(\theta) = I_m$ is determined by the intensity of the initial partial wave $\left|E_p^0\right|^2$ and the amplitude transmission coefficients a, t of the ring and the coupling region. The product at determines the fraction of the amplitude remaining in MRR after a single MRR transmission along with the coupling region. Therefore, the value $F = \pi\sqrt{at}/(1 - at)$ may be called the sharpness of MRR by analogy with the well-known Airy formula for the Fabry-Perot interferometer (FPI) [5], where instead of at the amplitude coefficient R is used. The amplitude E_p^0 is formed when optical energy is transferred from all longitudinal modes of the straight waveguide to the micro-ring resonator. It should be pointed out that in case when both waveguides are single-mode and the light attenuation in the coupling region is negligible, the ratios $E_p^0 = ikE_{in} = i\sqrt{1 - t^2}E_{in}$ and $I_m = I_{in} \cdot (1 - t^2)/(1 - at)^2$ are valid [9]. Calculation of k and I_m for the multi-mode waveguides requires taking into account the interaction of all longitudinal modes [12,14,19].

As noted above, the expression (8) in its physical meaning and structure corresponds to a similar expression for FPI. This allows us to use the formula for the loaded Q-factor of MRR at the wavelength λ_m use the formula

$$Q_{Airy} = \frac{\pi n_{gr}(\lambda_m) L_R}{2\lambda_m} / \arcsin\left(\frac{1 - at}{2\sqrt{at}}\right). \tag{9}$$

Here $n_{gr}(\lambda_m) = n_{\text{eff}} - \lambda_m \frac{dn_{\text{eff}}}{d\lambda}(\lambda_m)$ — the group refractive index ($n_{\text{eff}} = \beta_R/k_0$).

Thus, it is shown that for high-Q MRR with a given geometry and known optical parameters, the loaded Q-factor can be calculated by analogy with the formulas for FPI. If MRR is coupled with several waveguides, its Q-factor may also be calculated using formula (9) by replacing t with $\prod_i t_i$, where t_i — amplitude transmission coefficient of the i-th coupling section. To calculate the loaded Q-factor of MRR as part of the photonic integrated circuits, it is necessary to know the attenuation coefficient $\alpha(\lambda)$ in MRR or calculate $\alpha(\lambda)$ in terms of MRR transmission spectrum.

4. Q-factor calculation based on MRR transmission spectrum

The transmission spectrum of MRR samples in a photonic integrated circuit can be obtained using a radiation source that provides smooth tuning over a wide frequency range [20–22]. In this study, a high-resolution optical component analyzer HDCA 400 C+L was used to measure the Q-factor. (Fig. 5). The analyzer provides the ability to scan the spectrum in the wavelength range from 1520 to 1630 nm (in the frequency range from 184 to 197 THz). The transmission spectra of the samples for the two orthogonal polarizations were measured with a resolution of 0.0024 pm (0.3 MHz), which made it possible to calculate with high accuracy the Q-factor of the studied MRR that had widths of resonance curves greater than 3 pm (370 MHz). It shall be emphasized that the accuracy of frequency determination (wavelength) using the analyzer is ±0.5 pm (±62 MHz). Standards such as frequency combs [23,24], or high-precision calibration methods [25,26] may be used to improve measurement accuracy. All MRR samples are fabricated on one crystal [27] and have a typical geometry (Fig. 1). The waveguides for investigated photonic integrated circuit (PIC) have a S-shaped section (Fig. 5), which makes it possible to place the MRR samples on one crystal more densely. The distance between adjacent waveguides ensures that there is no coupling between the MRR samples and, consequently, an independent measurement of their transmission spectra. One of the measured transmission spectrum $T = P_{out}/P_{in}$ is shown in Fig. 6 (TE graph lies higher than TM graph). Dips in the transmission spectrum correspond to MRR resonances. The width and depth of each dip are determined by the values of the loaded and intrinsic Q-factor. The insert shows the same transmission spectrum in a narrow wavelength range.

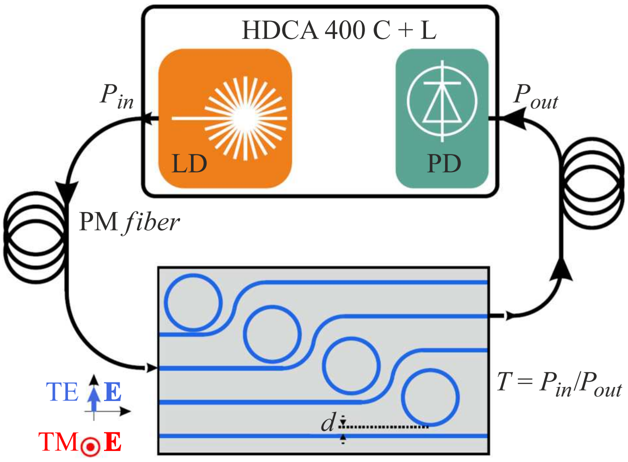

Figure 5. The scheme of the experimental setup for measurement of the transmission spectrum of MRR. LD — laser diode, PD — photodiode.

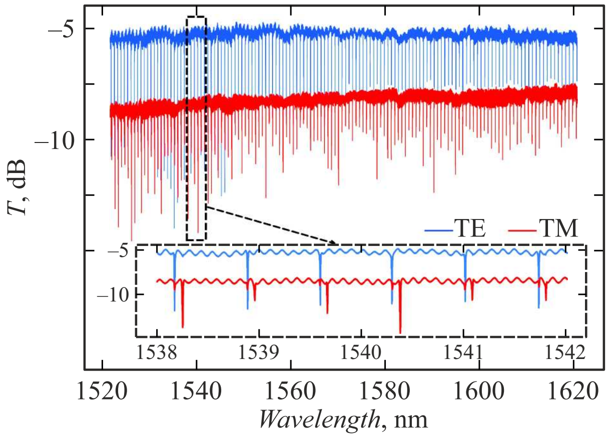

Figure 6. Experimentally measured transmission spectrum of a MRR sample as part of the photonic integrated circuit.

An approximating formula for the transmission spectrum is used to calculate the loaded Q-factor of MRR.

$$T = T_{FP} \cdot T_R,$$

$$T_R(\lambda) = \frac{a^2 - 2at \cdot \cos\theta + t^2}{1 - 2at \cdot \cos\theta + (at)^2}, \; \theta = 2\pi \cdot \frac{\lambda - \lambda_m}{\Delta\lambda_m},$$

$$T_{FP}(\lambda) = \frac{T_0}{1 + \frac{4\Gamma}{(1-\Gamma)^2} \sin^2\left(2\pi \cdot \frac{\lambda - \lambda_{FP}}{2 \cdot \Delta\lambda_{FP}}\right)}. \qquad (10)$$

Here T_R — transfer function of MRR [28]; $\Delta\lambda_m$ — the free spectral range of the MRR; T_{FP} — transfer function of the spurious FPI with the maximal value T_0, resonance wavelength λ_{FP}, free spectral range $\Delta\lambda_{FP}$ and reflectance coefficient Γ (in power), characterizing the reflectance from the edges of the photonic integrated circuit because of the absence of the anti-reflective coating [29]. It is assumed that the observed resonances correspond to the fundamental longitudinal modes of MRR, which are characterized by minimal attenuation in comparison with modes of higher orders. Each observed MRR resonance is approximated simultaneously with two neighboring resonances, assuming that the characteristics of $\Delta\lambda_m$, a, t are weakly dependent on the wavelength in the approximated window.

Figure 7 shows the transmission spectra for one of the MRR samples in two orthogonal polarizations in a window

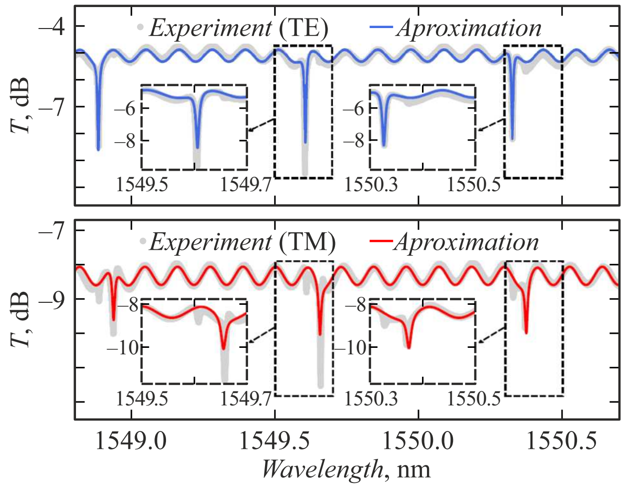

Figure 7. Example of approximation of the transmission spectrum $T(\lambda)$, dB.

with a width of ≈ 1.5 nm and the calculation results using the approximating function (10) with selected values of all parameters. The parameters are selected by minimizing the deviation of the model function from the experimental data using scipy.optimize (Python) software in two stages. First the parameters of T_{FP} function are selected, and further — values of parameters of T_R function.

Resonances at both polarizations are visible in each transmission spectrum. This can be explained by the rotation of the fiber tip, through which the laser diode radiation is introduced into the waveguides in PIC, which leads to the excitation of waveguide modes at both polarizations. The superposition of resonances of both polarizations is observed experimentally near the wavelength of 1560 nm for all the studied samples and reduces the accuracy of the approximation by the formula (10).

Figure 8 shows the values of the loaded Q-factor for four MRR samples, differing only in the gap d between the MRR and the straight waveguide. The values of the parameters a_e, t_e and n_{gr} found as a result of approximation of experimental data are used to calculate the experimental values of the loaded Q of MRR according to the formula (9). The obtained values are shown by symbols in Fig. 8. The model values of the loaded Q-factor (lines in Fig. 8) are calculated using the values of parameter a_e obtained from the experiment, as well as the calculated frequency

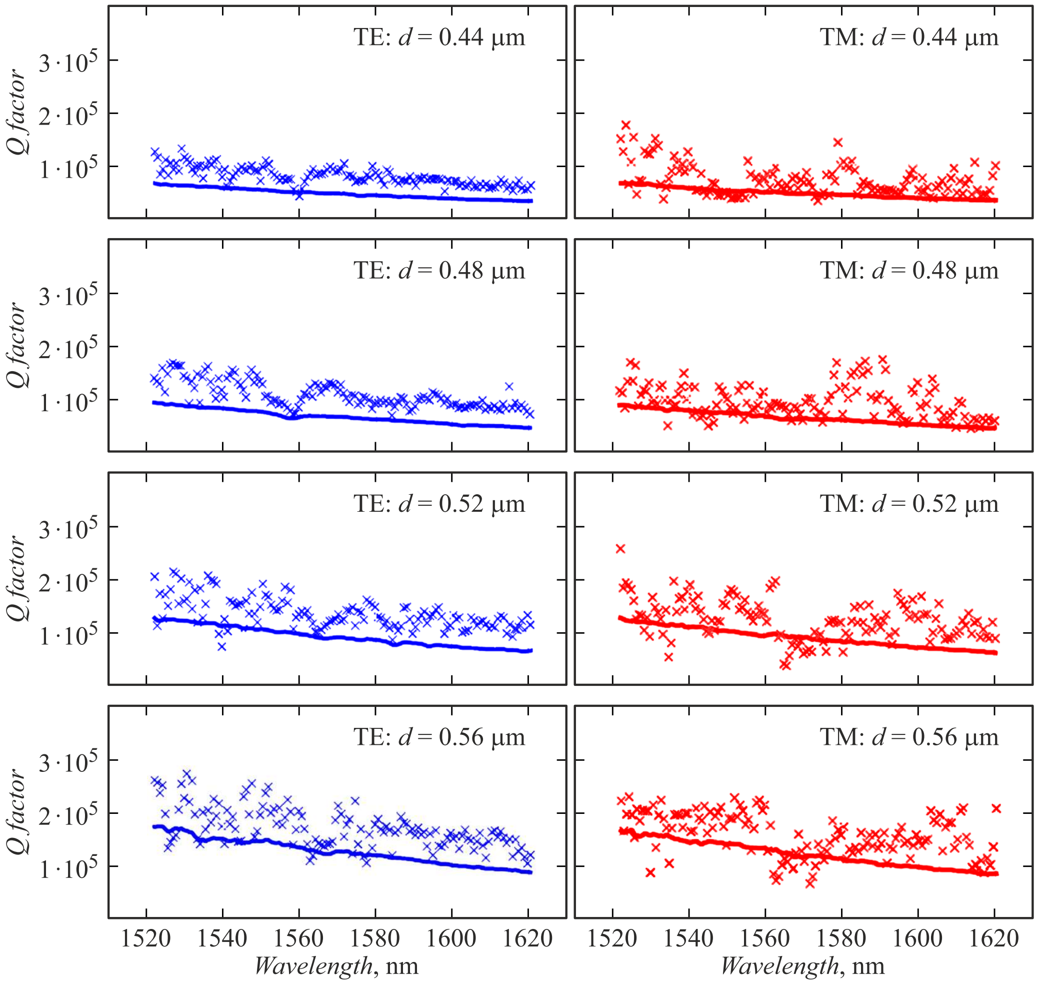

Figure 8. Experimental (crosses) and calculated (lines) of the loaded Q-factor of the studied MRR samples for TE- and TM-modes

dependence of the transmission coefficient t_c. The observed spread of experimental values of Q is caused by both the experimental error and the approximation inaccuracy.

It can be seen from the graphs that with increasing wavelength, the loaded Q-factor decreases. This is due to an increase in the size of the fundamental mode, the overlap integral (4) and a monotonous increase in losses in the coupling region — fraction of the power flowing from MRR into the waveguide. And with an increase in the gap d, the loaded Q-factor goes up, which is explained by lower losses in the coupling region (growth of parameter t). We may also see that the experimental and model values of the loaded Q-factor are close for the studied MRR samples, which indicates the proximity of the experimental and calculated values of parameter t (see (7)) — t_e and t_c respectively.

Conclusion

The sequence and methodology of simplified calculations of MRR characteristics are proposed. At the first stage, an easy-to-analyze description of the longitudinal modes of MRR and the straight section of the waveguide is presented. Then, based on the coupled-mode theory, the coupled coefficient of the MRR and straight waveguide is calculated. Obtained results and multipath interference method are used to find equation for the MRR transfer function. It is shown that MRR transmission spectrum can be approximated using Airy formula. It paves the way to calculate Q-factor in the same way as for the Fabry-Perot interferometer. At the final stage of Q-factor calculations, spectral dependences of the attenuation coefficient, obtained after processing the measured transmission spectra of MRR, are used. The loaded Q-factor of MRR as part of PIC was measured in the experiment. The obtained values are in good agreement with the calculated values. The adequacy of calculations confirmed by experiment allows to use the developed models for the design of high-Q MRR. The results obtained can be useful in the development of various linear and nonlinear devices based on the micro-ring resonators, for example, frequency comb generators, memory elements, etc. [4,30–34].

Funding

The research in St. Petersburg Electrotechnical University was funded by the Ministry of Science and Higher Education of the Russian Federation under Grant No. FSEE-2025-0014.

Conflict of interest

The authors declare that they have no conflict of interest.

References

[1] D.G. Rabus, C. Sada. *Integrated ring resonators* (Springer, Switzerland, 2020), DOI: 10.1007/978-3-030-60131-7

[2] A.A. Nikitin, V.V. Vitko, M.A. Cherkasskii, A.B. Ustinov, B.A. Kalinikos. Results in Phys., **18**, 103279 (2020). DOI: 10.1016/j.rinp.2020.103279

[3] T.J. Kippenberg, A.L. Gaeta, M. Lipson, M.L. Gorodetsky. Science, **361** (6402), (2018). DOI: 10.1126/science.aan8083

[4] X. Ji, S. Roberts, M. Corato-Zanarella, M. Lipson. APL Photon., **6**, 071101 (2021). DOI: 10.1063/5.0057881

[5] B. Saleh, M. Teich. *Optika i photonika. Printsipy i primeneniya* (Intellect, Dolgoprudniy, 2012) (in Russian)

[6] S. Sharma, S. Roy. J. Supercomput., **77**, 4332 (2021). DOI: 10.1007/s11227-020-03430-8

[7] A. Sveshnikov, A. Bogolyubov, A. Delitsyn, A. Krasilnikova, D. Minaev. Computers and Mathematics with Applications, **40** (12), 1387 (2000).
DOI: 10.1016/S0898-1221(00)00247-9

[8] H. Kogelnik. In: *Integrated Optics. Topics in Applied Physics*, ed. by T. Tamir (Springer, Berlin Heidelberg, 1975), DOI: 10.1007/978-3-662-43208-2_2

[9] A. Snyder, J. Love. *Teoriya opticheskikh volnovodov* (Radio i svyaz, M., 1987) (in Russian)

[10] A. Hardy, W. Streifer. J. Lightwave Technol., **3** (5), 1135 (1985). DOI: 10.1109/JLT.1985.1074291

[11] A. Hardy, W. Streifer. J. Lightwave Technol., **4** (1), 90 (1986). DOI: 10.1109/JLT.1986.1074633

[12] A. Hardy, W. Streifer, M. Osiński. Opt. Lett., **11**, 742 (1986). DOI: 10.1364/OL.11.000742

[13] V.F. Vzyatyshev, V.I. Kalinichev. Izv. vuzov. Radiofizika, **26** (4), 475 (1983) (in Russian).

[14] M.H. Pfeiffer, J. Liu, M. Geiselmann, T.J. Kippenberg. Phys. Rev. Appl., **7** (2), 024026 (2017).
DOI: 10.1103/PhysRevApplied.7.024026

[15] B. Mou, Y. Boxia, Q. Yan, W. Yanwei, H. Zhe, Y. Fan, W. Yu. Opt. Commun., **505**, 127437 (2022).
DOI: 10.1016/j.optcom.2021.127437

[16] M. Matsuhara, A. Watanabe. J. Opt. Soc. Am., **65**, 163 (1975). DOI: 10.1364/JOSA.65.000163

[17] D.R. Rowland, J.D. Love. IEE Proceedings J. (Optielectronics), **140** (3), 177 (1993).
DOI: 10.1049/ip-j.1993.0028

[18] M.L. Gorodetsky, V.S. Ilchenko. J. Opt. Soc. Am. B, **16** (1), 147 (1999). DOI: 10.1364/JOSAB.16.000147

[19] Z. Weissman, A. Hardy, E. Marom. Opt. Commun., **71** (6), 341 (1989). DOI: 10.1016/0030-4018(89)90045-X

[20] A.A. Ershov, A.I. Eremeev, A.A. Nikitin, A.B. Ustinov. Microwave Opt. Technol. Lett., **65** (8), 2451 (2023). DOI: 10.1002/mop.33675

[21] A.A. Nikitin, K.N. Chekmezov, A.A. Ershov, A.A. Semenov, A.B. Ustinov. Technical Physics, **69** (8), 1280 (2024). DOI: 10.61011/TP.2024.08.59017.72-24

[22] A.A. Ershov, K.N. Chekmezov, A.P. Burovikhin, A.A. Nikitin, S.N. Abolmasov, A.A. Stashkevich, E.I. Terukov, A.V. Eskov, A.A. Semenov, A.B. Ustinov. Izvestiya vuzov. Radioelektronika. **27** (2), 119 (2024) (in Russian).
DOI: 10.32603/1993-8985-2024-27-2-119-131

[23] P. Del'Haye, O. Arcizet, M.L. Gorodetsky, R. Holzwarth, T.J. Kippenberg. Nature Photonics, 3, 529 (2009). DOI: 10.1038/nphoton.2009.138

[24] J. Liu, G. Huang, R.N. Wang, J. He, A.S. Raja, T. Liu, N.J. Engelsen, T.J. Kippenberg. Nat. Commun., 12, 2236 (2021). DOI: 10.1038/s41467-021-21973-z

[25] N.Yu. Dmitriev, A.S. Voloshin, N.M. Kondratiev, V.E. Lobanov, K.N. Minkov, A.E. Shitikov, A. N. Danilin, E. A. Lonshakov, I.A. Bilenko. ZhETF, **162** (1), 14 (2022) (in Russian). DOI: 10.31857/S0044451022070021

[26] A.M. Mumlyakov, N.Yu. Dmitriev, M.V. Shibalov, I.A. Filippov, I.V. Trofimov, A.N. Danilin, V.E. Lobanov, I.A. Bilenko, M.A. Tarkhov. Phys. Rev. Appl., **22**, 054027 (2024). DOI: 10.1103/PhysRevApplied.22.054027

[27] M. Pfeiffer, A. Kordts, V. Brasch, M. Zervas, M. Geiselmann, J. Jost, T. Kippenberg. Optica, **3**, 20 (2016). DOI: 10.1364/OPTICA.3.000020

[28] V.N. Listvin, V.N. Treshchikov. *DWDM-sistemy* (Tekhnosfera, 2024) (in Russian).

[29] M. Poot, C. Schuck, X. Ma, X. Guo, H. Tang. Opt. Express, **24**, 6843 (2016). DOI: 10.1364/OE.24.006843

[30] S.S. Kosolobov, I.A. Pshenichnyuk, K.R Taziev, A.K. Zemtsova, D.S. Zemtsov, A.S. Smirnov, D.M. Zhigunov, V.P. Drachev. UFN, **194** (11), 1223 (2024) (in Russian). DOI: 10.3367/UFNr.2024.09.039762

[31] A.A. Nikitin, A.V. Kondrashov, V.V. Vitko, I.A. Ryabcev, G.A. Zaretskaya, N.A. Cheplagin, D.A. Konkin, A.A. Kokolov, L.I. Babak, A.B. Ustinov, B.A. Kalinikos. Opt. Commun., **480**, 126456 (2021). DOI: 10.1016/j.optcom.2020.12645

[32] A.A. Nikitin, I.A. Ryabcev, A.A. Nikitin, A.V. Kondrashov, A.A. Semenov, D.A. Konkin, A.A. Kokolov, F.I. Sheyerman, L.I. Babak, A.B. Ustinov. Opt. Commun., **511**, 127929 (2022). DOI: 10.1016/j.optcom.2022.127929

[33] N.M. Kondratiev, V.E. Lobanov, N.Y. Dmitriev, S.J. Cordette, I.A. Bilenko. Phys. Rev. A, **107** (6), 063508 (2023). DOI: 10.1103/PhysRevA.107.063508

[34] I. Kudelin, W. Groman, Q. Ji, J. Guo, M.L. Kelleher, D. Lee, T. Nakamura, C.A. McLemore, P. Shirmohammadi, S. Hanifi, H. Cheng, N. Jin, L. Wu, S. Halladay, Y. Luo, Z. Dai, W. Jin, J. Bai, Y. Liu, W. Zhang, C. Xiang, L. Chang, V. Iltchenko, O. Miller, A. Matsko, S.M. Bowers, P.T. Rakich, J.C. Campbell, J.E. Bowers, K.J. Vahala, F. Quinlan, S.A. Diddams. Nature, **627**, 534 (2024). DOI: 10.1038/s41586-024-07058-z

Translated by T.Zorina